

# Theoretical Study of Electronic-Structure for Semiconductor Quantum Dot

Ruhai Guo<sup>a</sup>, Hongyan Shi<sup>a</sup>, and Xiudong Sun<sup>a</sup>, Wisanu Pecharapa<sup>b</sup>, Wichan Techitdheera<sup>b</sup> and Jiti Nukeaw<sup>b</sup>

<sup>a</sup>Department of Applied Physics, Harbin Institute of Technology, Harbin 150001 People's Republic of China

<sup>b</sup>Department of Applied Physics, King Mongkut's Institute of Technology Ladkrabang, Bangkok 10520, Thailand

\* Corresponding author, E-mail: kpewisan@kmitl.ac.th

Received 16 May 2003

Accepted 7 Jan 2004

**ABSTRACT:** The electronic properties of self-assembled InAs/GaAs quantum dots are investigated theoretically. The ground-state transition energies for quantum dots in the shape of a cube, pyramid and “truncated pyramid” are calculated and analyzed. We use a method based on the Green's function technique for calculating strain in quantum dots and use an efficient plane-wave envelope-function technique to determine the ground-state electronic structure of the quantum dots having different shapes. Based on these results, we also calculated permanent built-in dipole moments and compared with recent experimental data. Our results demonstrate that the measured Stark effect in self-assembled quantum dot structures can be explained by including linear grading.

**KEYWORDS:** quantum dots, plane-wave expansion, self-assembled, quantum confined Stark effect.

## INTRODUCTION

Progress made in the growth of “free-standing” (e.g., colloidal) quantum dots and in the growth of semiconductor-embedded (“self-assembled”) dots has opened the door to new and exciting spectroscopic studies of quantum structures. The last decade has witnessed an intensive research effort focused on the physics of semiconductor quantum dots (QDs). Self-assembled InAs-GaAs quantum dots provide nearly ideal examples of zero-dimensional semiconductor systems<sup>1-4</sup> and are hence of considerable contemporary interest for the study of new physics and potential device applications. However, very little is known about their detailed atomic and electronic-structure, including, for instance, the form of the ground-state electron and hole wave functions. Therefore, to model and hence to control the optical and electronic properties, precise knowledge on a level as fundamental as the electronic-structure would be desirable. Initial structural studies of uncapped Stranski-Krastinow dots suggested a pyramidal shape,<sup>5</sup> and several groups therefore conducted theoretical investigations into the structure of ideal pyramidal dots.<sup>6-11</sup> The typical schematic diagram of an InAs pyramidal quantum dot and InAs wetting layer is as shown in Fig 1.

More recent structural study demonstrated that

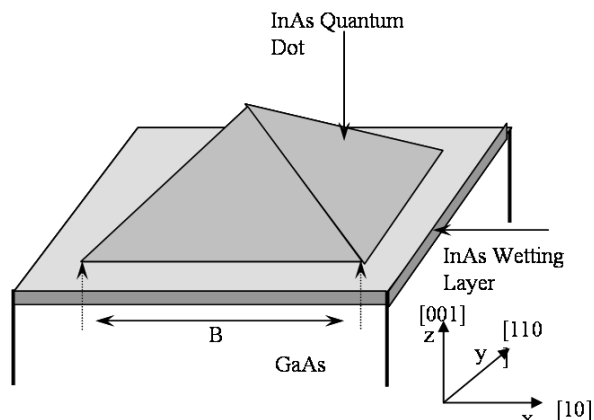


**Fig 1.** Schematic diagram of an InAs pyramidal quantum dot and InAs wetting layer together with axes referred to in the paper.

both the dot shape and size could vary with the growth conditions. In addition to the ideal pyramidal shape, more recent works have also provided evidence for “truncated” pyramids,<sup>12</sup> lens-shaped dots,<sup>13</sup> cone-shape dots,<sup>14</sup> as well as showing that In and Ga compositions can also vary through the dot.<sup>15-17</sup> These have revealed rich and sometimes unexpected features such as quantum-dot shape-dependent transitions, size-dependent (red) shifts between absorption and

emission, emission from high excited levels, surface-mediated transitions, exchange splitting, strain-induced splitting, and Coulomb-blockade transitions. These new results have promoted the need for developing suitable theoretical tools capable of analyzing the electronic structure of quantum dots.

The first theoretical study of the electronic properties of these structures used the single-band effective-mass theory to calculate the energy levels and wave functions in InAs/GaAs cone-shape quantum dots.<sup>14</sup> The strain was taken to be a constant in the InAs material and zero in the surrounding GaAs barrier. More recently, the single-band theory was used for InAs/GaAs dots with a more realistic pyramidal geometry.<sup>5</sup> The variations of the strain in and around the InAs island were determined using elastic continuum theory, in which the atomic nature of the constituent materials was neglected. Both approaches neglected valence-band mixing, and the strain dependence of the effective masses. Figures in most theoretical papers on ideal pyramidal dots show the presence of a permanent dipole in the dot, due to the large built-in strain fields which localize the highest energy hole state near the bottom of the pyramid. Therefore, it sits underneath the lowest-energy electron state in the dot. Because of the built-in dipole, QD structures should exhibit an asymmetric Stark shift in the presence of an applied field. As an electric field  $F$  is applied, the transition energy  $E_{TR}$  between the ground-state electron and hole levels will vary quadratically as  $E_{TR}(F) = E_{TR}(0) - pF + \beta F^2$ , where  $E_{TR}(0)$  is the zero-field transition energy,  $p$  depends on the built-in dipole, and  $\beta$  is a measure of the polarizability of the electron and hole wave functions. Asymmetry in experimental measurements of the Stark shift has indeed revealed a built-in dipole both in InAs/GaAs,<sup>18</sup> and also in Al<sub>y</sub>In<sub>1-y</sub>As/Al<sub>x</sub>Ga<sub>1-x</sub>As quantum dots but, surprisingly, the direction of the dipole is opposite to that predicted from the theoretical calculations, with the hole center of mass above the electron center of mass in both cases. Some recent theoretical works have explained this “inverted” alignment by assuming composition grading in the pyramidal InAs QDs.<sup>16,17</sup>

In this paper, we use a theoretical investigation of different shape and size influencing the sign and magnitude of the built-in dipole in QDs with cubic, pyramidal and “truncated” pyramidal shapes. Here we consider three kinds of common shapes of quantum dots with constant composition, and show whether these can lead to the correct sign in the built-in dipole moment, compared to that observed experimentally. The calculations were undertaken using separate one-band Hamiltonian equation for the electrons and holes. We also present a simple method for calculating strain

fields in quantum dots, but neglecting anisotropy. As result of our work, we show conclusively that the measured Stark effect in self-assembled quantum dot structures can be explained by including linear grading.

## MATERIALS AND METHODS

The calculations were performed for a three-dimensional superlattice of dots, with superlattice unit cell size  $2B_x \times 2B_y \times 2B_z$ . A Schrödinger equation for the system was solved using a plane-wave envelope-function technique. The normalized envelope wave functions  $\Psi_n(\vec{r})$  are determined using a Fourier series expansion

$$\Psi_n(\vec{r}) = \sum_{\vec{k}} \frac{A_{\vec{k}}^n}{\sqrt{8B_x B_y B_z}} \exp(i\vec{k} \cdot \vec{r}), \quad (1)$$

where  $\vec{k} = \pi(m/B_x, n/B_y, p/B_z)$  and  $\vec{r} = (x, y, z)$ . We choose the separation between neighboring dots to be equal to the dot dimension in order to minimize cross interaction, while also ensuring efficient convergence of the Fourier series. We first describe here the general method and then discuss the particular form of the strained one-band Hamiltonian equations used. The Schrödinger equation here is

$$\hat{H}\Psi_n = E_n\Psi_n \quad (2)$$

Using the plane-wave basis, we substitute (2) with (1) and then leaving  $\frac{1}{\sqrt{8B_x B_y B_z}} \exp(-i\vec{k}' \cdot \vec{r})$  for integration under periodic boundary condition. The energy levels and eigenfunctions were found by solving the large Hamiltonian matrix equation

$$\sum_{\vec{k}} \bar{H}_{\vec{k},\vec{k}'} A_{\vec{k}}^n = E_n A_{\vec{k}'}^n, \quad (3)$$

$$\bar{H}_{\vec{k},\vec{k}'} = \int_{\vec{r}} \frac{d\vec{r}}{8B_x B_y B_z} \exp(-i\vec{k}' \cdot \vec{r}) H(\vec{r}) [\exp(i\vec{k} \cdot \vec{r})]. \quad (4)$$

In order to set up the Hamiltonian matrix of Eq. (3), we must first evaluate the matrix elements  $\bar{H}_{\vec{k},\vec{k}'}$  linking plane-wave basis states of wave vector  $\vec{k}$  and  $\vec{k}'$ . The misfit of lattice constant of the quantum dot material will generate a non-uniform strain distribution throughout the dot and the matrix. Both the electron and hole Hamiltonian equations contain terms depending on this local strain distribution. The calculation of the spatial strain distribution in a QD structure requires the solution of a three-dimensional problem in elasticity theory. This is often achieved by using finite-difference or atomistic technologies,<sup>8,19</sup> which require considerable computational effort. A method based on the Green's function technique for calculating strain in quantum dot structures was recently presented.<sup>20</sup> An analytical formula in the form

of a Fourier series has been obtained for the strain tensor for arrays of QDs of arbitrary shape taking account the anisotropy of elastic properties. Of equal or greater importance, the technique is also particularly well-suited as input for electronic structure calculations based on the envelope function method using a plane-wave expansion technique, because the strain-dependent matrix element linking any pair of the plane waves can be determined analytically. We use this approach to directly determine the strain-dependent terms in the Hamiltonian matrix. We assume for simplicity that the dot and matrix elastic constants are equal and isotropic, with the values given in Table 1.

We derive the electron and hole envelope function Hamiltonian equations from one-band  $\bar{k} \cdot \bar{P}$  theory.<sup>21,22</sup> The electron Hamiltonian is given as

$$\hat{H}_c(\bar{r}) = -\frac{\hbar^2}{2m_0^*(\bar{r})}\nabla^2 + V_c + a_c\epsilon_{hy}(\bar{r}) + d_{pz}(\bar{r}) + eFz, \quad (5)$$

where  $m^*(\bar{r})$  is the electron effective mass,  $V_c$  the unstrained conduction-band edge,  $a_c\epsilon_{hy}(\bar{r})$  the hydrostatic deformation of the conduction band edge, and  $d_{pz}(\bar{r})$  the piezoelectric potential. The strain-induced band deformation causes the effective-mass parameters to vary from their bulk values. The variation of the electron effective mass with the (hydrostatically) strained band gap,  $E_{gs}$ , is given as

$$\frac{1}{m^*(\bar{r})} = 1 + \frac{2E_p(\bar{r})}{3E_{gs}(\bar{r})} + \frac{E_p(\bar{r})}{3[E_{gs}(\bar{r}) + \Delta_0(\bar{r})]} + \delta(\bar{r}) \quad (6)$$

where  $E_p(\bar{r})$  is the Kane interband energy parameter,  $\delta(\bar{r})$  takes into account the contribution of remote bands to the conduction-band effective mass, and  $\Delta_0(\bar{r})$  is the spin-orbit splitting energy.

Substituting Eq. (5) into Eq. (4), the expression for  $\bar{H}_{\bar{k},\bar{k}'}$  has the form

$$\bar{H}_{\bar{k},\bar{k}'} = \frac{1}{8B_x B_y B_z} \int_r d\bar{r} \exp(i\bar{k}'' \cdot \bar{r}) \left[ \frac{\hbar^2}{2m_0^*} (k_x''^2 + k_y''^2 + k_z''^2) + V_c + a_c\epsilon_{hy}(\bar{r}) + d_{pz}(\bar{r}) + eFz \right] \quad (7)$$

where  $\bar{k}'' = \bar{k} - \bar{k}'$ . We define the characteristic function of the dot  $\chi(\bar{r})$  in the supercell (1 for InAs, 0 for GaAs), and take the lattice mismatch of the dot to be 6.7% for InAs in GaAs. It can be shown for an isotropic elastic medium that the Fourier transform of the real-space strain tensor component  $\epsilon_{ij}(\bar{r})$  is given by ( $\bar{k}'' \neq 0$ ),<sup>20</sup>

$$\tilde{\epsilon}_{ij}(\bar{k}'') = \epsilon_0 \tilde{\chi}(\bar{k}'') \left[ \delta_{ij} - \frac{3\lambda + 2\mu}{\lambda + 2\mu} \frac{k_i'' k_j''}{|\bar{k}''|^2} \right], \quad (8)$$

where  $\lambda = C_{12}$  and  $\mu = C_{44}$  are the Lamé constants for an isotropic elastic medium.  $\chi(\bar{k}'')$  is the Fourier transform

**Table 1.** Parameters used in this paper.

Parameters	InAs	GaAs
$\gamma_1^I$	19.67	6.85
$\gamma_2^I$	8.37	2.1
$E_g$	0.418eV	1.519eV
$\Delta_0$	0.38eV	0.33eV
$E_p$	22.2eV	25.7eV
$m_{exp}^*$ (0 K)	0.023	0.067
$a_c$	-5.08	-7.17
$a_v$	1.00	1.16
$e_{14}^v/\epsilon_0 \times 10^{-3} \text{cm}^{-2}$	-2.97	-12.49
$V_c$ (300 K)	0.621eV	1.428eV
$V_v$	0.265eV	0.000eV
$V_c + a_c \epsilon_{hy}$ (300 K)	0.994eV	1.428eV
$V_v + a_v \epsilon_{hy}$	0.192eV	0.000eV
$C_{11}$	$11.9 \times 10^{10} \text{Pa}$	
$C_{12}$	$5.38 \times 10^{10} \text{Pa}$	
$C_{44}$	$5.95 \times 10^{10} \text{Pa}$	
$b_{ax}$	1.8eV	
$\epsilon_t(\text{InAs})$	15.15	

of the dot characteristic function.

For the case of isotropic elastic constants, evaluation of the analytic form of  $\bar{H}_{\bar{k},\bar{k}'}$  is a trivial matter for all but the piezoelectric term in  $\hat{H}_c(\bar{r})$ . In order to evaluate this term, we use the analytic expression of Ref. 23 for the Fourier transform of the piezoelectric potential ( $\bar{k}'' \neq 0$ ),

$$\bar{d}_{pz}(\bar{k}'') = \frac{-18i\epsilon_0}{\alpha_0 \sqrt{2\pi}} \left( \frac{C_{11} + 2C_{12}}{C_{11}} \right) \left[ \frac{e_{14}^{bar} \chi(\bar{k}'') k_x'' k_y'' k_z''}{\alpha_r^{bar} |\bar{k}''|^4} + \left( \frac{e_{14}^{dot}}{\alpha_r^{dot}} - \frac{e_{14}^{bar}}{\alpha_r^{bar}} \right) \sum_{k''} \chi(\bar{k}'' - \bar{k}'') \chi(\bar{k}'') \frac{k_x'' k_y'' k_z''}{|\bar{k}''|^4} \right], \quad (9)$$

where  $\alpha_0$ ,  $\alpha_r^{dot}$  and  $\alpha_r^{bar}$  are the permittivity of free space and relative permittivity of the dot and barrier material, respectively.  $e_{14}^{dot}$  and  $e_{14}^{bar}$  are the piezoelectric constants.

From experiment, Stranski-Krastanow quantum dots have a large base-to-height ratio. The kinetic energy in the x-y plane is thus reduced relative to that in the growth direction, leading to stronger heavy-hole confinement and weaker light-hole confinement. The one-band valence Hamiltonian we use for the hole ground state is then given as

$$\hat{H}_v(\bar{r}) = -\frac{\hbar^2}{2m_0} \{ [\gamma_1(\bar{r}) + \gamma_2(\bar{r})] \nabla_{||}^2 + [\gamma_1(\bar{r}) - 2\gamma_2(\bar{r})] \nabla_z^2 \} + V_v + a_v \epsilon_{hy}(\bar{r}) - b_{ax} \epsilon_{ax}(\bar{r}) + d_{pz}(\bar{r}) + eFz \quad (10)$$

where  $V_v$  is the unstrained valence band-edge energy,  $a_v \epsilon_{hy}(\bar{r})$  the hydrostatic deformation of the valence-band edge, and  $-b_{ax} \epsilon_{ax}(\bar{r})$  the axial-strain-induced shift in the heavy-hole band edge. In a similar way, we can

obtain the Hamiltonian matrix  $\bar{H}_{\vec{k},\vec{k}}$  for the valence band. The following calculations were carried out assuming room temperature energy gaps and effective masses. In order to correctly describe the one-band Luttinger parameters  $\gamma_i(\bar{r})$ , we first relate them to their eight-band counterparts,  $\gamma'_i(\bar{r})$ . In the full eight-band Hamiltonian, the interactions between the conduction-band minimum and valence-band maximum are considered explicitly, with  $\gamma'_i(\bar{r})$  then due to interactions with remote bands, and assumed to be independent of the built-in strain and the lowest-energy gap. The eight-band  $\gamma'_i(\bar{r})$  values are related to the one-band values by<sup>24,25</sup>

$$\gamma'_1(\bar{r}) = \gamma_1(\bar{r}) - \frac{E_p(\bar{r})}{3E_g(\bar{r})}, \gamma'_2(\bar{r}) = \gamma_2(\bar{r}) - \frac{E_p(\bar{r})}{6E_g(\bar{r})}, \quad (11)$$

where  $E_g$  is the unstrained band gap. The energy gap changes in a strained material, so that the one-band Luttinger parameters will also change in a strained inclusion, as

$$\gamma_1(\bar{r}) = \gamma'_1(\bar{r}) + \frac{E_p(\bar{r})}{3E_g(\bar{r})}, \gamma_2(\bar{r}) = \gamma'_2(\bar{r}) + \frac{E_p(\bar{r})}{6E_g(\bar{r})}. \quad (12)$$

The parameters used are tabulated in Table 1. We calculated the parameter values for InAs in a GaAs matrix, and for unstrained GaAs. We obtained strain-normalized one-band effective masses of  $\gamma_1=10.601$ ,  $\gamma_2=3.253$ , and  $m^*=0.042$ . Finally, we assume the GaAs values for the elastic constants in the dot and surrounding matrix. This assumption has been justified previously, based on Key's scaling rule for elastic constants.<sup>20</sup>

## RESULTS AND DISCUSSION

In Fig 2(a and b), we give the variation of the ground-state electron and hole confinement energies, and calculate different shapes of quantum dots as a function of dot size, with a base to height ratio of 2:1. The results for pyramidal quantum dots are in good agreement with previous calculations.<sup>6,9</sup> We also calculate ground-state confinement energies for "truncated" pyramidal quantum dots and cuboidal quantum dots and find that electron and hole confinement energies become closer as the quantum dots become flatter. We defined truncation factor  $f$  as the bottom part of a full pyramid of height  $2B_z/(1-f)$ . The conduction-band spacing is in the order of 100 meV between cuboidal and "truncated" pyramidal quantum dots, and 150 meV between "truncated" pyramidal and pyramidal quantum dots. It can be explained that symmetry of the QD shape takes great effect to the quantum-confined ground energy of electron. The hole spacings are much

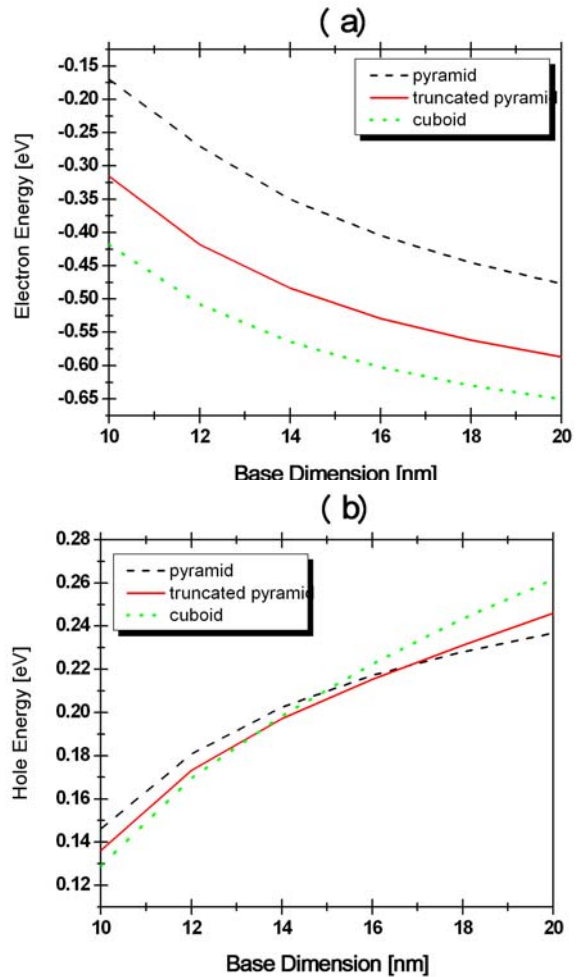
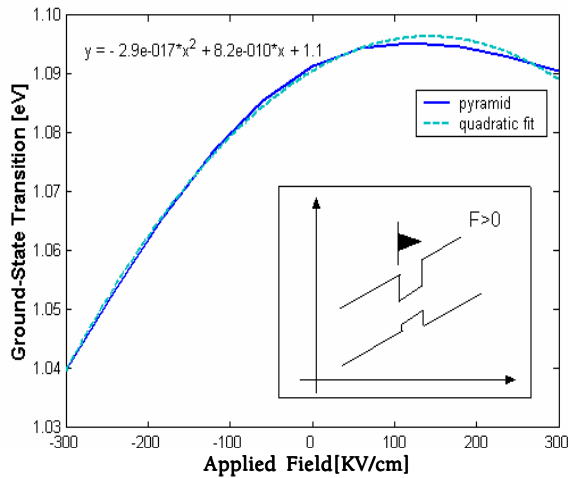


Fig 2. Ground-state electron and hole confinement energies (300 K) as a function of dot size for InAs quantum dots of base: height ratio 2:1, pyramidal quantum dots (dashed line), "truncated" pyramidal quantum dots (solid line), "truncated" pyramidal quantum dots (truncated factor  $f=0.75$ ) (solid line), and cuboidal quantum dots (dotted line).

smaller due to their higher effective mass. Fig 3 shows the calculated difference between the electron and hole ground state energies for the dot structure considered in Fig 1 when the electric field is applied along the z-axis. We have defined the applied field to be positive when it results in the conduction- and valence-band edges moving to higher energy above the dot and to lower energy below the dot, as illustrated in Fig 3.

It can be seen that the transition energy varies quadratically with the applied field, so that  $E_{TR}(F) = E_{TR}(0) - pF + \beta F^2$ . The linear coefficient  $p$  depends directly on the initial separation of the electron and hole mean positions, i.e., on the built-in ground-state dipole moment of the dot. The peak transition



**Fig 3.** Ground-state transition energy (300K) as a function of applied field for pyramidal dots having base width 12 nm and height 6 nm. The solid line shows the theoretical calculation and the dashed line shows the quadratic fit to it. Insert: variation of the band edge with position for  $F > 0$ .

energy is seen at positive field in Fig 3, consistent with a negative dipole moment. Using quadratic fit in Fig 3, we get the dipole  $d = -p/e$ , with  $d = -8.2\text{\AA}$ . By contrast, experimental Stark shift measurements both on InAs/GaAs and  $\text{In}_x\text{Ga}_{1-x}\text{As}/\text{Al}_x\text{Ga}_{1-x}\text{As}^{18}$  QD structures show the peak transition energy at negative fields. The experimentally observed built-in dipole is therefore of opposite sign to that predicted from Fig 3, with the hole-electron separation  $d = 4.0 \pm 1\text{\AA}$  in Ref. 18.

We therefore conclude that the structure of these buried Stranski-Krastinow-grown dots must be largely different from an ideal constant composition pyramid, and now turn to consider which dot structures are consistent with the experimentally observed sign in the dipole. Fig 4 shows the calculated dipole in a “truncated” pyramidal dots of base width  $B=18$  nm and height  $H=5.5$  nm as a function of “truncated” factor,  $f$ . The value assumed for  $H$  is similar to the value estimated from a TEM analysis of uncapped dots.<sup>18</sup>  $f$  represents the fraction of the total pyramid height removed so that the height of the full pyramid is 22 nm. Changing from a cuboidal to a pyramidal geometry, the increasing anisotropy of the dot shape modifies the axial strain fields to move the heavy hole more rapidly away from the top surface of the dot and toward the dot base than the ground-state electron, and the magnitude of the electron-hole separation increases. If the hole is to sit in the upper part of the dot, above the electron, we require a deeper heavy-hole potential at the top of the dot than at the base. The heavy-hole potential can then be deeper at the top than at the base if the dot is formed from an  $\text{In}_x\text{Ga}_{1-x}\text{As}$  alloy, with indium composition,  $x$ , increasing from base to top. We have assumed a linear

composition gradient, but recent work suggests that the true composition profile may be more complicated. The solid line shows a linear graded cuboid, for which  $d=0$  when  $x=1$  at the base, with the  $d$  increasing to a maximum value  $\sim 7\text{\AA}$  near  $x \sim 0.3$  at the base. A similar trend is observed for the “truncated” pyramid with  $f=0.75$  (dashed line). We see from Fig 4, the correct sign of dipole can be obtained by including the composition gradient. We have omitted the influence of the wetting

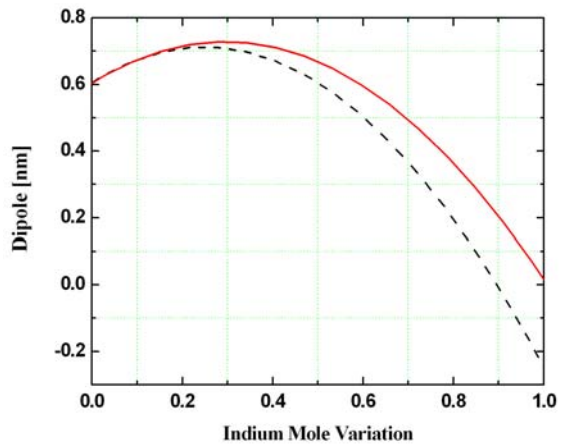


**Fig 4.** Dipole (300 K) as a function of composition gradient for dots of base width of 18nm and height of 5.5 nm, graded from  $\text{In}_x\text{Ga}_{1-x}\text{As}$  at the base to InAs at the top of the surface. The solid line are results for cuboidal dots and the dashed lines are results for “truncated” pyramidal dots ( $f=0.75$ ).

layer from calculation because the grading must be stronger in the presence of the wetting layer.

### CONCLUSION

In this article, we have used an efficient plane-wave envelope-function technique to determine the ground-state electronic structure of dots with three types of shape. We have presented a method based on a Green’s function approach to calculate strain distributions in QDs. We have noted that this calculation method is also particularly appropriate as an input step in calculations of the electronic structures of quantum dots. We have used one-band electron and hole Hamiltonian equations to investigate the different factors influencing the magnitude and sign of the built-in dipole in strained quantum dots. We have demonstrated that the built-in strain will always lead to the hole center of mass lying below the electron center of mass in a constant composition dot with common shapes. The calculated dipole moment is of the opposite sign to that determined from the recent quantum-confined Stark effect experimental measurements. Our results demonstrate

conclusively that the measured Stark effect in self-assembled quantum dots with different shapes and fixed compositions can be explained theoretically by including composition gradients.

## ACKNOWLEDGEMENTS

The authors would like to give thanks to Department of Applied Physics, King Mongkut's Institute of Technology Ladkrabang (Bangkok) for financial support.

## REFERENCES

1. Weller H and Eychmüller A (1996) *Semiconductor Nanoclusters*, (Edited by Kamat PV and Meisel D), Vol. 103, **5**, Elsevier, New York.
2. Overbeek JTG (1982) Monodisperse colloidal systems, fascinating and useful. *Adv Colloid I Sci* **15**, 251-77.
3. Seifert W, Carlson N, Miller M, Pistol ME, Samuelson L, and Wallenberg L (1966) In-situ growth of quantum dot structures by stranski-krastanow growth mode. *Prog Cryst Growth Charact* **33**, 423-71.
4. Tabuchi M, Noda S, and Sasaki A (1992) *Science and Technology of Microscopic Surfaces*, (Edited by Namba S, Hamaguchi C, and Ando T), pp379. Springer, Tokyo.
5. Grundmann M, Stier O, and Bimberg D (1995) InAs/GaAs pyramidal quantum dots: Strain distribution, optical phonons, and electronic structure. *Phys Rev B* **52**, 11969-81.
6. Stier O, Grundmann M, and Bimberg D (1999) Electronic and optical properties of strained quantum dots modeled by 8-band k-p theory. *Phys Rev B* **59**, 5688-701.
7. Williamson AJ and Zunger A (1999) InAs quantum dots: Predicted electronic of free-standing versus GaAs-embedded structures. *Phys Rev B* **59**, 15819-24.
8. Cusack MA, Briddon PR, and Jaros M (1996) Electronic structure of InAs/GaAs self-assembled quantum dots. *Phys Rev B* **54**, R2300-3.
9. Cusack MA, Briddon PR, and Jaros M (1998) Electronic structure, impurity binding energies, absorption spectra of InAs/GaAs quantum dots. *Physica B* **253**, 10-27.
10. Chang K and Xia JB (1997) Asymmetric stark shifts of exciton in InAs/GaAs pyramidal quantum dots. *Solid State Commun.* **104**, 351-4.
11. Ruvimov S, Werner P, Sheerschmidt K, Gösele U, Heydenreich J, Richter U, Ledentsov NN, Grundmann M, et al (1995) Structural characterization of (In,Ga)As quantum dots in a GaAs matrix. *Phys Rev B* **51**, 14766-9.
12. Ledentsov NN, Shchukin VA, Grundmann M, Kirstaedter N, Bimberg D, Ustinov VM, Egorov AY, Zhukov AE, et al (1996) Direct formation of vertically coupled quantum dots in Stranski-Krastanow growth. *Phys Rev B* **54**, 8743-50.
13. Moison JM, Houzay F, Barthe F, Leprince L, André E, and Vatel O (1994) Self organized growth of regular nanometer-scale InAs dots on GaAs. *Appl Phys Lett* **64**, 196-8.
14. Marzin JY, Bastard G (1994) Calculation of the energy levels in InAs/GaAs quantum dots. *Solid State Commun* **92**, 437-42.
15. Kegel I, Metzger TH, Fratzi P, Peisl J, Lorke A, Garcia JM, and Petroff PM (1999) Interdependence of strain and shape in self-assembled coherent InAs islands on GaAs. *Europhys Lett* **45**, 222-7.
16. Liu N, Tersoff J, Baklenov O, Holmes AL Jr., and Shih CK (2000) Non-uniform composition profile in  $\text{In}_{0.5}\text{Ga}_{0.5}\text{As}$  Alloy quantum dots. *Phys Rev Lett* **84**, 334-7.
17. Sheng W and Leburton JP (2001) Electron-hole alignment in InAs/GaAs self-assembled quantum dots: Effects of chemical composition and dot shape. *Phys Rev B* **63**, 161301(R).
18. Fry PW, Itskevich IE, Mowbray DJ, Skolnick MS, Finley JJ, Barker JA, O'Reilly EP, Wilson LR, et al (2000) Inverted electron-hole alignment in InAs-GaAs self-assembled quantum dots. *Phys Rev Lett* **84**, 733-6.
19. Benabbas T, Francois P, Androussi Y, and Lefebvre A (1996) Stress relaxation in highly strained InAs/GaAs structures as studied by finite element analysis and transmission electron microscopy. *J Appl Phys* **80**, 2763-7.
20. Andreev AD, Downes JR, Faux DA, and O'Reilly EP (1999) Strain distributions in quantum dots of arbitrary shape. *J Appl Phys* **86**, 297-305.
21. Barker JA and O'Reilly EP (1999) The influence of interdiffusion on electron states in quantum dots. *Physica E* **4**, 231-7.
22. Bastard G (1980) *Wave Mechanics Applied to Semiconductor Heterostructures*. Halstead Press, New York.
23. Davies JH (1998) Elastic and piezoelectric fields around a buried quantum dot: A simple picture. *J Appl Phys* **84**, 1358-65.
24. Pidgeon CR and Brown RN (1966) Interband magnetoabsorption and Faraday Rotation in InSb. *Phys Rev* **146**, 575-83.
25. Meney AT, Gonul B, and O'Reilly EP, (1994) Evaluation of various approximations used in the envelope-function method. *Phys Rev B* **50**, 10893-904.